







## Joint User Localization and Location Calibration of a Hybrid Reconfigurable Intelligent Surface

Reza Ghazalian , *Member, IEEE*, Hui Chen , *Member, IEEE*,  
George C. Alexandropoulos , *Senior Member, IEEE*,  
Gonzalo Seco-Granados , *Fellow, IEEE*,  
Henk Wymeersch , *Senior Member, IEEE*,  
and Riku Jäntti , *Senior Member, IEEE*

**Abstract**—The recent research in the emerging technology of reconfigurable intelligent surfaces (RISs) has identified its high potential for localization and sensing. However, to accurately localize a user placed in the area of influence of an RIS, the RIS location needs to be known a priori and its phase profile is required to be optimized for localization. In this article, we study the problem of the joint localization of a hybrid RIS (HRIS) and a user, considering that the former is equipped with a single reception radio-frequency (RF) chain enabling simultaneous tunable reflections and sensing via power splitting. Focusing on the downlink of a multi-antenna base station, we present a multi-stage approach for the estimation of the HRIS position and orientation as well as the user position. Our simulation results, including comparisons with the Cramér-Rao lower bounds, demonstrate the efficiency of the proposed localization approach, while showcasing that there exists an optimal HRIS power splitting ratio for the desired multi-parameter estimation problem.

**Index Terms**—Channel estimation, hybrid reconfigurable intelligent surface, localization, sensing, synchronization.

### I. INTRODUCTION

Reconfigurable intelligent surfaces (RISs) consist of multiple meta-materials of an almost passive nature [1], which can impact the characteristics of electromagnetic (EM) waves impinging on them, such as the phase, offering radio propagation control [2]. The RIS-parameterized channel can assist communications via its potential beamforming gain and act as an additional passive anchor in improving localization performance [3]. Therefore, reconfigurable intelligent surfaces (RISs) are considered as a candidate technology for the sixth generation (6G) of wireless systems [4], [5], where joint localization and communication are expected to support various use cases [6], such as autonomous driving, digital twins, and other immersive applications. The consideration of RISs for localization applications has received significant

Manuscript received 2 October 2022; revised 28 April 2023; accepted 9 August 2023. Date of publication 21 August 2023; date of current version 17 January 2024. This work was supported in part by the Academy of Finland Profi-5 under Grant 326346, in part by ULTRA under Grant 328215, in part by EU H2020 RISE-6G Project under Grant 10101701, in part by ICREA Academia Program, and in part by Spanish R+D project under Grant PID2020-118984GB-I00. The review of this article was coordinated by Dr. Balasubramaniam Natarajan. (Corresponding author: Reza Ghazalian.)

Reza Ghazalian and Riku Jäntti are with the Department of Communications and Networking, School of Electrical Engineering of Electrical Engineering, Aalto University, 02150 Espoo, Finland (e-mail: ghazalian66@gmail.com; riku.jantti@aalto.fi).

Hui Chen and Henk Wymeersch are with the Department of Electrical Engineering, Chalmers University of Technology, 412 58 Gothenburg, Sweden (e-mail: hui.chen@chalmers.se; henkw@chalmers.se).

George C. Alexandropoulos is with the Department of Informatics and Telecommunications, National and Kapodistrian University of Athens, 15784 Athens, Greece (e-mail: alexandg@di.uoa.gr).

Gonzalo Seco-Granados is with the Department of Telecommunications and Systems Engineering, Universitat Autònoma de Barcelona, 08193 Barcelona, Spain (e-mail: gonzalo.seco@uab.cat).

Digital Object Identifier 10.1109/TVT.2023.3306936

attention in recent years, see, e.g., [7], [8], [9], [10], [11], [12]. In [7], [8], [9], [10], [11], [12], two-dimensional (2D) and 3D user localization scenarios with either a far-field (FF) or near-field (NF) channel model, static or mobility conditions, as well as single-input-single-output or multiple-input-multiple-output (MIMO) system setups were considered to showcase the potential of RIS-assisted localization.

In the RIS-focused research, channel estimation is a challenging problem due to the cascaded channel structure between the base station (BS) and the user equipment (UE), as well as the commonly considered passive nature of RISs, which deprives them from any estimation capability. Nevertheless, the various available cascade channel estimation techniques [13], [14] result in certain limitations on the wireless operation design [15] (the lack of the individual channels complicates network management and the design of modulation and coding) and challenge wireless localization [16], since a cascade channel estimation does not decouple the AOA/AOD at the RIS. In addition, the vast majority of the RIS-based localization studies [7], [8], [9], [10], [11], [12], [17] assume that the RIS state (mainly its position and orientation) is known, which can be nontrivial in various practical cases. The estimation of the RIS state was only recently addressed in [18], however, the locations of both transmitters and receivers were assumed known, which requires certain overhead for infrastructure calibration. As a consequence, the high-accuracy joint location estimation of UEs and RISs is an open problem.

One of the main challenges with the latter estimation problem stems from the fact that the angle of arrival (AOA) and angle of departure (AOD) at the RIS are coupled and cannot be estimated separately. For instance, the authors in [19] have estimated the only sinusoidal value of the difference between AOA and AOD at the RIS.<sup>1</sup> It is worthwhile mentioning that having knowledge about the AOA and AOD is essential to estimate the RIS rotation angles. To tackle this issue, in this article, we propose the adoption of an RIS equipped with a single reception (RX) radio-frequency (RFC) chain, instead of using a passive RIS. This RIS architecture, which was first presented in [20] to enable the estimation of individual channels and was then extended in [15] to hybrid RISs capable of simultaneous reflection and sensing, considers wave-guides capable of feeding the impinging signals at each RIS unit element to base-band unit via a network of phase shifters which combines them to feed an RX RFC chain. We particularly consider an HRIS and focus on its joint localization with a UE in a 2D scenario under FF conditions. A multi-stage estimator is presented whose performance is benchmarked by the Cramér-Rao lower bounds (CRBs). Our simulation results demonstrate the efficiency of the proposed estimation approach and showcase the impact of the HRIS power splitting ratio on the localization performance.

**Notation:** Vectors and matrices are indicated by lowercase and uppercase bold letters, respectively. Notation  $[\mathbf{A}]_{i,j}$  represents  $\mathbf{A}$ 's element in the  $i$ -th row and  $j$ -th column, while the index  $i : j$  determines all the elements between  $i$  and  $j$ . The complex conjugate, Hermitian, transpose, and Moore-Penrose inverse operators are represented by  $(\cdot)^*$ ,  $(\cdot)^H$ ,  $(\cdot)^T$ , and  $(\cdot)^\dagger$ , respectively.  $\|\cdot\|$  returns the norm of vectors or the Frobenius norm of matrices, whereas  $\odot$  and  $\otimes$  indicate the element-wise and Kronecker products, respectively.  $\mathbf{1}_K$  is a column vector comprising all ones with length  $K$  and function  $\text{atan2}(y, x)$  is the four-quadrant inverse tangent function.

<sup>1</sup>Having knowledge about the AOA at the BS to the RIS and AOA at the UE from the RIS [19], is not enough to estimate the RIS position with an unknown UE position.

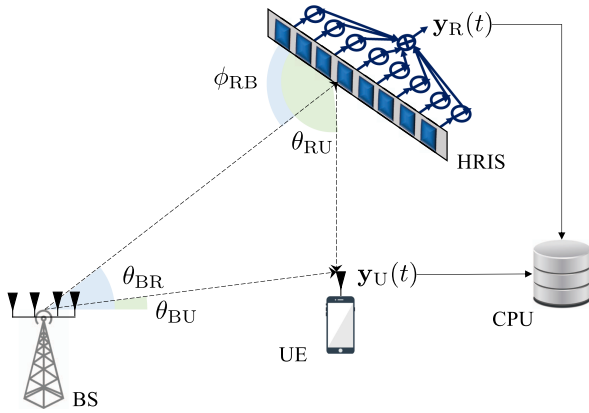


Fig. 1. Considered scenario including a single-RX-RF HRIS, whose power splitting ratio and phase shifting network are controlled by a digital controller.

## II. SYSTEM AND CHANNEL MODELS

### A. System Setup

Consider the wireless system scenario in Fig. 1 operating in the mm-Wave frequency band and consisting of one  $M_B$ -antenna BS with a known location  $\mathbf{p}_B \in \mathbb{R}^2$ , one single-antenna UE with an unknown location  $\mathbf{p}_U \in \mathbb{R}^2$ , and an HRIS with unknown location  $\mathbf{p}_R \in \mathbb{R}^2$  and an orientation angle  $\alpha$ . We focus on the downlink direction considering that the BS sends  $T$  orthogonal frequency division multiplexing (OFDM) symbols over time via  $N_c$  subcarriers. We assume that all associated channels remain constant during each transmission interval. We use the matrix  $\mathbf{R}_\alpha = [[\cos \alpha, \sin \alpha]^\top, [-\sin \alpha, \cos \alpha]^\top]$  to represent the rotation that maps the global frame of reference to the coordinate system associated with the HRIS. Moreover, the HRIS and UE are assumed not to be synchronized with the BS, leading to the unknown clock biases  $b_R$  and  $b_U$  at the HRIS and UE, respectively, with respect to the BS. Thus, besides the HRIS position and UE location, the clock bias of these components needs to be estimated.<sup>2</sup>

We further assume that the UE operates in the FF range of the BS and the HRIS. The BS is equipped with a uniform linear array (ULA), whose  $m$ -th element, with  $m = 0, 1, \dots, M_B - 1$ , is located at the point  $[\delta_B(2m - M_B + 1)/2, 0]^\top$ , where  $\delta_B$  denotes the spacing between adjacent antenna elements. Accordingly, we define the global coordinate system to be aligned with local coordinate system at the BS. The HRIS is a ULA with  $M_R$  unit elements attached to a single RX RF chain [15], [20], enabling the reception of the impinging signal. The  $\ell$ -th element, with  $\ell = 0, 1, \dots, M_R - 1$ , of HRIS is located at the point (in the HRIS local coordinate system)  $[\delta_R(2\ell - M_R + 1)/2, 0]^\top$ , where  $\delta_R$  is the space between two adjacent meta-elements. For the sake of simplicity, we assume that  $\delta_R = \delta_B = \delta = \lambda/2$ , with  $\lambda$  being the wavelength of the central carrier frequency. We finally make the common assumption [14] that the HRIS and the UE share their observations with a central processing unit (CPU), being responsible to carry out the targeted joint estimation that will be presented in the sequel, via a reliable link.

<sup>2</sup>Note that the HRIS and LOS are necessary to solve this joint calibration and localization problem. Using a passive RIS makes the problem unsolvable because the AOA and AOD at RIS cannot be decoupled. Without HRIS, the problem is not solvable. Similarly, LOS is mandatory for delay estimation due to the existence of synchronization errors between HRIS, UE, and BS.

### B. Models for the Received Signals and Channels

As shown in Fig. 1, the HRIS structure includes  $M_R$  identical power splitters [15], which divide the received signal power at each element into two parts: one for reflection and the other for sensing/reception. For the latter operation, to feed a portion of the impinging signal to the single RX RF chain, the HRIS applies,<sup>3</sup> a combining vector modeled by  $\mathbf{c}_t \in \mathbb{C}^{M_R \times 1}$  with  $|\mathbf{c}_t[i]| = 1$  during each time interval  $t$ , choosing for discrete Fourier transform (DFT) codebook [21]. The HRIS also changes its phase profile in discrete time slots, to reflect signals towards the UE. We use the vector  $\boldsymbol{\gamma}_t \in \mathbb{C}^{M_R \times 1}$ , with  $|\boldsymbol{\gamma}_t[k]| = 1$ , to represent the HRIS reflection phase profile at each time  $t$ . For the multi-antenna BS, we also adopt the DFT for its beamforming vector  $\mathbf{f}_t \in \mathbb{C}^{M_B \times 1}$  at each time instant  $t$  [21], and consider unit-power symbols for transmission. Under the latter assumptions and after removing the cyclic prefix and taking the fast Fourier transform (FFT), the received OFDM symbols during each  $t$ -th time interval, with  $t = 1, 2, \dots, T$ , at the HRIS and the UE, which are respectively denoted as  $\mathbf{y}_R(t) \in \mathbb{C}^{N_c \times 1}$  and  $\mathbf{y}_U(t) \in \mathbb{C}^{N_c \times 1}$ , can be expressed as follows:<sup>4</sup>

$$\mathbf{y}_R(t) = g_{BR} \sqrt{\rho P_t} \mathbf{d}(\tau_{BR}) \mathbf{c}_t^\top \mathbf{a}_R(\phi_{RB}) \mathbf{a}_B^\top(\theta_{BR}) \mathbf{f}_t + \mathbf{w}_R(t), \quad (1)$$

$$\mathbf{y}_U(t) = \mathbf{y}_{BU}(t) + \mathbf{y}_{BRU}(t) + \mathbf{w}_U(t), \quad (2)$$

where  $\mathbf{y}_{BU} \in \mathbb{C}^{N_c \times 1}$  and  $\mathbf{y}_{BRU} \in \mathbb{C}^{N_c \times 1}$  represent the received signals at the UE from the BS through the line of sight (LOS) and reflected paths, respectively, which are given by:

$$\mathbf{y}_{BU}(t) = g_{BU} \sqrt{P_t} \mathbf{d}(\tau_{BU}) \mathbf{a}_B^\top(\theta_{BU}) \mathbf{f}_t, \quad (3)$$

$$\mathbf{y}_{BRU}(t) = g_{BRU} \sqrt{(1-\rho)P_t} \mathbf{d}(\tau_{BRU}) \mathbf{a}_B^\top(\theta_{RU}) \text{diag}(\boldsymbol{\gamma}_t) \mathbf{a}_R(\phi_{RB}) \mathbf{a}_B^\top(\theta_{BR}) \mathbf{f}_t, \quad (4)$$

where  $\rho$  is the common power splitting ratio at the power splitters, while  $g_{BU}$ ,  $g_{BR}$ , and  $g_{BRU}$  denote the unknown complex gains of the BS-UE, BS-HRIS, and BS-HRIS-UE wireless links, respectively, which are modeled as  $g_i \triangleq |g_i| e^{-j\phi_i}$  with  $i \in \{BR, BU, BRU\}$ , where  $\phi_i \sim \mathcal{U}[0, 2\pi)$  and  $|g_i|$  follows the model described in [18]. The delay steering vector  $\mathbf{d}(\tau)$  in the latter expressions is defined as:

$$\mathbf{d}(\tau) \triangleq [1, e^{-j2\pi\Delta f\tau}, \dots, e^{-j2\pi(N_c-1)\Delta f\tau}]^\top, \quad (5)$$

where  $\Delta f$  denotes the sub-carrier spacing. Based on the lack-of-synchronization assumption and the location of the different components of the system, we can express the propagation delay for all links as follows:

$$\tau_{BR} = \frac{d_{BR}}{c} + b_R, \quad \tau_{BU} = \frac{d_{BU}}{c} + b_U, \quad \tau_{BRU} = \frac{d_{BR} + d_{RU}}{c} + b_U, \quad (6)$$

where  $d_{BR} \triangleq \|\mathbf{p}_B - \mathbf{p}_R\|$ ,  $d_{BU} \triangleq \|\mathbf{p}_B - \mathbf{p}_U\|$ , and  $d_{RU} \triangleq \|\mathbf{p}_R - \mathbf{p}_U\|$  with  $c$  being the speed of light.

In addition,  $\theta_{BR}$  and  $\theta_{BU}$  respectively represent the AODs from the BS towards the HRIS and the UE, based on the BS local coordinate system. In fact, the angles  $\theta_{BR}$  and  $\theta_{BU}$  are along the directions of the vectors  $\mathbf{q}_{BR} \triangleq (\mathbf{p}_R - \mathbf{p}_B) / \|\mathbf{p}_R - \mathbf{p}_B\|$  and  $\mathbf{q}_{BU} \triangleq (\mathbf{p}_U - \mathbf{p}_B) / \|\mathbf{p}_U - \mathbf{p}_B\|$ , respectively. Similarly,  $\theta_{RU}$  and  $\phi_{RB}$  are the AOD from the HRIS to the

<sup>3</sup>A dedicated phase-shifting network feeds the impinging signals at all the HRIS elements to the single RX RF chain. It is assumed that the central processing unit knows both the HRIS combining vector and phase profile.

<sup>4</sup>For the sake of simplicity, we ignore the effects of scatter points (SPs) on the received signals, since their channels are weak compared to the HRIS channel. Nevertheless, we study how they affect our proposed estimator in our simulations.

UE and the AOA to the HRIS from the BS both in the HRIS local coordinate system, respectively. Accordingly, one can write  $\theta_{\text{RU}} = \text{atan2}([\mathbf{q}_{\text{RU}}]_2, [\mathbf{q}_{\text{RU}}]_1)$  and  $\phi_{\text{RB}} = \text{atan2}([\mathbf{q}_{\text{RB}}]_2, [\mathbf{q}_{\text{RB}}]_1)$ , where  $\mathbf{q}_{\text{RU}} \triangleq \mathbf{R}_{\alpha}(\mathbf{p}_{\text{U}} - \mathbf{p}_{\text{R}}) / \|\mathbf{p}_{\text{U}} - \mathbf{p}_{\text{R}}\|$  and  $\mathbf{q}_{\text{RB}} \triangleq \mathbf{R}_{\alpha}(\mathbf{p}_{\text{B}} - \mathbf{p}_{\text{R}}) / \|\mathbf{p}_{\text{B}} - \mathbf{p}_{\text{R}}\|$ . Finally, in (1) and (2), the steering vectors at the BS ( $\mathbf{a}_{\text{B}}(\nu) \in \mathbb{C}^{M_{\text{B}} \times 1}$ ) and the HRIS ( $\mathbf{a}_{\text{R}}(\nu) \in \mathbb{C}^{M_{\text{R}} \times 1}$ ) are defined as follows:

$$\mathbf{a}_{\text{B}}(\nu) = \left[ e^{j \frac{\pi \sin \nu (M_{\text{B}} - 1)}{2}}, \dots, 1, \dots, e^{-j \frac{\pi \sin \nu (M_{\text{B}} - 1)}{2}} \right]^{\top}, \quad (7a)$$

$$\mathbf{a}_{\text{R}}(\nu) = \left[ e^{j \frac{\pi \sin \nu (M_{\text{R}} - 1)}{2}}, \dots, 1, \dots, e^{-j \frac{\pi \sin \nu (M_{\text{R}} - 1)}{2}} \right]^{\top}, \quad (7b)$$

where  $\nu$  shows the AOD at the BS to the HRIS and UE or AOA/AOD at the HRIS from/to the BS/UE.  $P_t$  denotes the transmitted power, and  $\mathbf{w}_{\text{R}} \in \mathbb{C}^{N_c \times 1}$  and  $\mathbf{w}_{\text{U}} \in \mathbb{C}^{N_c \times 1}$  represents the additive thermal noise vectors at the HRIS and the UE, respectively, each containing zero-mean circularly-symmetric independent and identically distributed Gaussian elements with variance  $\sigma^2 = N_0 N_c \Delta f$ , where  $N_0$  is noise power spectral density.

### III. PROPOSED MULTI-PARAMETER ESTIMATION

In this article, capitalizing on the received signal models in (1) and (2), we focus on the estimation of the unknown channel parameters included in the vector  $\boldsymbol{\zeta} \triangleq [\boldsymbol{\eta}_{\text{ch}}^{\top}, g_{\text{BR}}, g_{\text{BU}}, g_{\text{BRU}}]^{\top}$ , where  $\boldsymbol{\eta}_{\text{ch}} \triangleq [\boldsymbol{\tau}^{\top}, \boldsymbol{\theta}^{\top}, \phi_{\text{RB}}]^{\top}$  with  $\boldsymbol{\tau} \triangleq [\tau_{\text{BR}}, \tau_{\text{BU}}, \tau_{\text{BRU}}]^{\top}$  and  $\boldsymbol{\theta} \triangleq [\theta_{\text{BR}}, \theta_{\text{BU}}, \theta_{\text{RU}}]^{\top}$ , as well as the state parameters in the vector  $\boldsymbol{\zeta}_{\text{s}} \triangleq [\mathbf{p}_{\text{R}}^{\top}, \alpha, \mathbf{p}_{\text{R}}^{\top}, b_{\text{R}}, b_{\text{U}}]^{\top}$ . We next present a multi-stage estimation approach that is based on the relationship derived in Section II-B between the channel and state parameters.

#### A. BS-HRIS Channel Estimation

We commence by estimating the TOA at the HRIS. To this end, we stack all  $T$  observations via (1) in the matrix  $\mathbf{Y}_{\text{R}}^0 \in \mathbb{C}^{N_c \times T}$ , yielding:

$$\mathbf{Y}_{\text{R}}^0 = g_{\text{BR}} \sqrt{\rho P_t} \mathbf{d}(\tau_{\text{BR}}) \mathbf{a}_{\text{R}}^{\top} + \mathbf{W}_{\text{R}}^0, \quad (8)$$

where  $\mathbf{a}_{\text{R}} \triangleq \boldsymbol{\Omega}^{\top} \text{vec}(\mathbf{a}_{\text{R}}(\phi_{\text{RB}}) \mathbf{a}_{\text{B}}^{\top}(\theta_{\text{BR}}))$ ,  $\boldsymbol{\Omega} \triangleq [\mathbf{f}_1 \otimes \mathbf{c}_1, \dots, \mathbf{f}_T \otimes \mathbf{c}_T] \in \mathbb{C}^{M_{\text{B}} M_{\text{R}} \times T}$ , and  $\mathbf{W}_{\text{R}}^0 \in \mathbb{C}^{N_c \times T}$  includes the noise contribution at the HRIS over all sub-carrier and time slots. We then compute the FFT of each column of  $\mathbf{Y}_{\text{R}}^0$  followed by integration over time (i.e., taking the absolute value squared of the FFT output) to estimate  $\tau_{\text{BR}}$ . For this, we use the method proposed in [9]. Then, we eliminate the effect of  $\tau_{\text{BR}}$  performing the calculation  $\mathbf{Y}_{\text{R}}^0 \odot (\mathbf{d}(-\hat{\tau}_{\text{BR}}) \mathbf{1}_T^{\top})$ . Taking the sum over the subcarriers and after some algebraic manipulations, the following expression is deduced:<sup>5</sup>

$$\mathbf{y}_{\text{R}}^1 = g_{\text{BR}} \sqrt{\rho P_t} N_c \boldsymbol{\Omega}^{\top} \mathbf{A}_{\text{R}}(\phi_{\text{RB}}) \mathbf{a}_{\text{B}}(\theta_{\text{BR}}) + \mathbf{w}_{\text{R}}^1, \quad (9)$$

where  $\mathbf{y}_{\text{R}}^1 \in \mathbb{C}^{T \times 1}$ ,  $\mathbf{w}_{\text{R}}^1 \triangleq (\mathbf{W}_{\text{R}}^0)^{\top} \odot (\mathbf{1}_T \mathbf{d}(-\hat{\tau}_{\text{BR}})^{\top}) \mathbf{1}_{N_c}$ , and  $\mathbf{A}_{\text{R}}(\phi_{\text{RB}}) \triangleq (\mathbf{I}_{M_{\text{B}}} \otimes \mathbf{a}_{\text{R}}(\phi_{\text{RB}}))$ . Using this expression and based on noisy measurement, i.e.,  $\mathbf{y}_{\text{R}}^1$ , we can obtain the estimates for  $g_{\text{BR}}$ ,  $\theta_{\text{BR}}$ , and  $\phi_{\text{RB}}$  via solving the maximum likelihood (ML) problem:

$$\left[ \hat{g}_{\text{BR}}, \hat{\theta}_{\text{BR}}, \hat{\phi}_{\text{RB}} \right] = \arg \min_{g_{\text{BR}}, \theta_{\text{BR}}, \phi_{\text{RB}}} \left\| \mathbf{y}_{\text{R}}^1 - g_{\text{BR}} \sqrt{\rho P_t} N_c \boldsymbol{\Omega}^{\top} \mathbf{A}_{\text{R}}(\phi_{\text{RB}}) \mathbf{a}_{\text{B}}(\theta_{\text{BR}}) \right\|^2. \quad (10)$$

<sup>5</sup>We ignored delay estimation errors and approximated the model to facilitate algorithm development. If the algorithm attains the CRB, we then obtain a sufficiently accurate approximate model. Otherwise, residual errors will occur if the model is incorrect, and one must refine the algorithm. However, we will see in the simulation results that the proposed estimator attains the corresponding CRB at the high transmit power, showing the approximation's correctness.

To solve the latter optimization problem, we introduce the unstructured vector<sup>6</sup>  $\mathbf{v} \triangleq g_{\text{BR}} \sqrt{\rho P_t} N_c \mathbf{a}_{\text{B}}(\theta_{\text{BR}})$ , which is a function of unknown parameters, i.e.,  $g_{\text{BR}}$  and  $\theta_{\text{BR}}$ . We first estimate  $\phi_{\text{RB}}$  via the following minimization problem:

$$\hat{\phi}_{\text{RB}} = \arg \min_{\phi_{\text{RB}}} \left\| \mathbf{y}_{\text{R}}^1 - \boldsymbol{\Omega}^{\top} \mathbf{A}_{\text{R}}(\phi_{\text{RB}}) \mathbf{v}(\phi_{\text{RB}}) \right\|^2, \quad (11)$$

where  $\mathbf{v}(\phi_{\text{RB}}) = (\boldsymbol{\Omega}^{\top} \mathbf{A}_{\text{R}}(\phi_{\text{RB}}))^\dagger \mathbf{y}_{\text{R}}^1$  represents the estimate of  $\mathbf{v}$  as a function of  $\phi_{\text{RB}}$ . The solution of (11) can be obtained through a line search over  $\phi_{\text{RB}}$ . Considering (9) and (11), we can also estimate  $\theta_{\text{BR}}$  via the minimization:

$$\hat{\theta}_{\text{BR}} = \arg \max_{\theta_{\text{BR}}} \left\| \mathbf{y}_{\text{R}}^1 - g_{\text{BR}}(\theta_{\text{BR}}) \beta \boldsymbol{\Omega}^{\top} \mathbf{A}_{\text{R}}(\hat{\phi}_{\text{RB}}) \mathbf{a}_{\text{B}}(\theta_{\text{BR}}) \right\|^2, \quad (12)$$

where  $\beta \triangleq \sqrt{\rho P_t} N_c$  and  $g_{\text{BR}}$  can be expressed as a function of  $\theta_{\text{BR}}$  as  $g_{\text{BR}}(\theta_{\text{BR}}) = (\beta \boldsymbol{\Omega}^{\top} \mathbf{A}_{\text{R}}(\hat{\phi}_{\text{RB}}) \mathbf{a}_{\text{B}}(\theta_{\text{BR}}))^\dagger \mathbf{y}_{\text{R}}^1$ . Note that, one can solve (12) via a line search over  $\theta_{\text{BR}}$ . All in all, by applying  $\hat{\phi}_{\text{RB}}$  and  $\hat{\theta}_{\text{BR}}$  obtained in (11) and (12), respectively, as the method's initial points, we use Newton's method to refine the estimation of  $\theta_{\text{BR}}$  and  $\phi_{\text{RB}}$  considering (10). The required gradients are computed from (10) by basic calculus.

#### B. Estimation of the BS-UE and BS-HRIS-UE Channels

We assume that the received power at the UE from the BS is much larger than that from the HRIS, which facilitates us to first estimate the BS-UE channel.<sup>7</sup> Based on this assumption as well as on (2) and (3), we can approximate the received signal at the UE as follows:

$$\mathbf{Y}_{\text{U}}^0 \approx g_{\text{BU}} \sqrt{P_t} \mathbf{d}(\tau_{\text{BU}}) \mathbf{a}_{\text{B}}^{\top}(\theta_{\text{BU}}) \mathbf{F} + \mathbf{W}_{\text{BU}}^0, \quad (13)$$

where  $\mathbf{F} \triangleq [\mathbf{f}_1, \mathbf{f}_2, \dots, \mathbf{f}_T]$  and  $\mathbf{W}_{\text{BU}}^0 \in \mathbb{C}^{N_c \times T}$  includes the noise contribution at the UE over all subcarriers and time slots. We take a similar approach to that before to estimate  $\tau_{\text{BU}}$ . After removing the effect of this TOA and integrating the signals over the  $N_c$  subcarrier frequencies, the noisy observations is deduced as:

$$\mathbf{y}_{\text{U}}^0 = g_{\text{BU}} \sqrt{P_t} N_c \mathbf{F}^{\top} \mathbf{a}_{\text{B}}(\theta_{\text{BU}}) + \mathbf{w}_{\text{BU}}^0, \quad (14)$$

where  $\mathbf{y}_{\text{U}}^0 \in \mathbb{C}^{T \times 1}$  and  $\mathbf{w}_{\text{BU}}^0 \triangleq (\mathbf{W}_{\text{BU}}^0)^{\top} \odot (\mathbf{1}_T \mathbf{d}(-\hat{\tau}_{\text{BU}})^{\top}) \mathbf{1}_{N_c}$ . The parameter  $\theta_{\text{BU}}$  can be estimated by solving the following problem via a simple line search:

$$\hat{\theta}_{\text{BU}} = \arg \min_{\theta_{\text{BU}}} \left\| \mathbf{y}_{\text{U}}^0 - g_{\text{BU}}(\theta_{\text{BU}}) \sqrt{P_t} N_c \mathbf{F}^{\top} \mathbf{a}_{\text{B}}(\theta_{\text{BU}}) \right\|^2, \quad (15)$$

where  $g_{\text{BU}}(\theta_{\text{BU}}) \triangleq (\sqrt{P_t} N_c \mathbf{F}^{\top} \mathbf{a}_{\text{B}}(\theta_{\text{BU}}))^\dagger \mathbf{y}_{\text{U}}^0$ . The problem (15) can be solved through line search over  $\theta_{\text{BU}}$ . This coarse estimate can be used as the initial point in Newton's method, as described before.

By using the BS-UE channel estimation, we can recover the LOS signal received at the UE from the BS and, consequently, remove its contribution from the received signal. However, it is critical to note that one needs to estimate the LOS channel parameters with high accuracy, otherwise, they will affect the estimation of the NLOS channel parameters. We proceed by defining the matrix:

$$\mathbf{Y}_{\text{U}}^1 \approx g_{\text{BRU}} \sqrt{(1 - \rho) P_t} \mathbf{d}(\tau_{\text{BRU}}) \mathbf{a}^{\top}(\theta_{\text{RU}}, \hat{\theta}_{\text{BR}}, \hat{\phi}_{\text{RB}}) \boldsymbol{\Xi} + \mathbf{W}_{\text{BRU}}^0, \quad (16)$$

<sup>6</sup>The goal of introducing unstructured vector  $\mathbf{v}$  is to reduce the complexity of 2D search over  $\theta_{\text{BR}}$  and  $\phi_{\text{RB}}$  search space for solving (10). We transform the 2D problem (joint estimate of the  $\theta_{\text{BR}}$  and  $\phi_{\text{RB}}$ ) into 2 one-dimensional problems, i.e.,  $\phi_{\text{RB}}$  estimate and  $\theta_{\text{BR}}$  estimate problems.

<sup>7</sup>For scenarios where the HRIS has large dimensions, a certain condition in the time evolution of the phase profile has been imposed [15]. This can be adopted to cancel the effect of the HRIS channel, and hence, assist in the channel estimation process.



where  $\Xi \triangleq [\mathbf{f}_1 \otimes \gamma_1, \dots, \mathbf{f}_T \otimes \gamma_T]$ ,  $\mathbf{W}_{\text{BRU}}^0 \in \mathbb{C}^{N_c \times T}$ , and

$$\mathbf{a}(\theta_{\text{RU}}, \hat{\theta}_{\text{BR}}, \hat{\phi}_{\text{BR}}) \triangleq \text{vec}((\mathbf{a}_{\text{R}}(\theta_{\text{RU}}) \odot \mathbf{a}_{\text{R}}(\hat{\phi}_{\text{RB}})) \mathbf{a}_{\text{B}}^{\top}(\hat{\theta}_{\text{BR}})). \quad (17)$$

It is noted that the adoption of the HRIS allows us to estimate the AOA and AOD at the HRIS side, which would be impossible in the case of a passive RIS. Similarly to above, after removing the effect of  $\tau_{\text{BRU}}$  from (16) and integrating over all sub-carrier frequencies, we can obtain the expression:

$$\mathbf{y}_{\text{U}}^1 = \tilde{g} \Xi^{\top} \mathbf{a}(\theta_{\text{RU}}, \hat{\theta}_{\text{BR}}, \hat{\phi}_{\text{RB}}) + \mathbf{w}_{\text{BRU}}^0, \quad (18)$$

where  $\tilde{g} \triangleq g_{\text{BRU}} \sqrt{(1-\rho)P_t N_c}$  and  $\mathbf{w}_{\text{BRU}}^0 \triangleq (\mathbf{W}_{\text{BRU}}^0)^{\top} \odot (\mathbf{1}_T \mathbf{d}(-\hat{\tau}_{\text{BRU}})^{\top}) \mathbf{1}_{N_c}$ . Hence, the estimation for angle  $\theta_{\text{RU}}$  can be obtained from the following minimization:

$$\hat{\theta}_{\text{RU}} = \arg \min_{\theta_{\text{RU}}} \|\mathbf{y}_{\text{U}}^1 - \tilde{g}_{\text{BRU}}(\theta_{\text{RU}}) \Xi^{\top} \mathbf{a}(\theta_{\text{RU}}, \hat{\theta}_{\text{BR}}, \hat{\phi}_{\text{RB}})\|^2, \quad (19)$$

with  $\tilde{g}_{\text{BRU}}(\theta_{\text{RU}}) \triangleq (\Xi^{\top} \mathbf{a}(\theta_{\text{RU}}, \hat{\theta}_{\text{BR}}, \hat{\phi}_{\text{RB}}))^{\dagger} \mathbf{y}_{\text{U}}^1$ , using a simple line search. As before, this coarse estimation of  $\hat{\theta}_{\text{RU}}$  can be used as the initial point of the Newton's method for solving the ML optimization problem (19).

### C. State Estimation

In this step, the state parameters are estimated using the previously estimated parameters. We make use of the one-to-one mapping presented in Section II-B between the channel and state parameters. We specifically use expression (6) to define the following parameter:

$$\hat{d} \triangleq d_{\text{BR}} + d_{\text{RU}} - d_{\text{BU}} = c(\hat{\tau}_{\text{BRU}} - \hat{\tau}_{\text{BU}}). \quad (20)$$

Based on the triangular shape formulated by the system nodes in Fig. 1, we can write  $\sin(\beta_0)/d_{\text{RU}} = \sin(\beta_1)/d_{\text{BU}} = \sin(\beta_2)/d_{\text{BR}}$ , where  $\angle\beta_0 = |\hat{\theta}_{\text{BR}} - \hat{\theta}_{\text{BU}}|$ ,  $\angle\beta_1 = |\hat{\phi}_{\text{RB}} - \hat{\theta}_{\text{RU}}|$ , and  $\angle\beta_2 = \pi - \angle\beta_0 - \angle\beta_1$ . From (20) and considering the law of sines, the distances from the BS to the other two network nodes can be computed as:

$$\hat{d}_{\text{BU}} = \frac{\hat{d} \sin \beta_1}{\sin \beta_0 + \sin \beta_2 - \sin \beta_1}, \quad \hat{d}_{\text{BR}} = \frac{\hat{d} \sin \beta_2}{\sin \beta_0 + \sin \beta_2 - \sin \beta_1}. \quad (21)$$

Using these expressions and the AODs from the BS to the other two nodes, the positions of the HRIS and UE can be estimated as  $\hat{\mathbf{p}}_{\text{R}} = \mathbf{p}_{\text{B}} + \hat{d}_{\text{BR}} \cos \hat{\theta}_{\text{BR}}$  and  $\hat{\mathbf{p}}_{\text{U}} = \mathbf{p}_{\text{B}} + \hat{d}_{\text{BU}} \cos \hat{\theta}_{\text{BU}}$ , respectively. We can also estimate the clock bias at the HRIS and UE as  $\hat{b}_{\text{R}} = \hat{\tau}_{\text{BR}} - \hat{d}_{\text{BR}}/c$  and  $\hat{b}_{\text{U}} = \hat{\tau}_{\text{BU}} - \hat{d}_{\text{BU}}/c$ , respectively. Based on the relationship between the AOA at the HRIS from the BS and the AOD from the BS to the HRIS, one can finally estimate the HRIS orientation as  $\hat{\alpha} = \pi - \hat{\theta}_{\text{BR}} - \hat{\phi}_{\text{RB}}$ .

### D. Complexity Analysis of the Proposed Estimator

We analyze the computational complexity of the proposed estimator, dominated by channel parameters estimation. In the first step for each channel estimation, we calculate 2D NF-point DFT for delay estimation, with  $\mathcal{O}(N_F \log(N_F))$  computational complexity. For the angle estimation, we assume that the search intervals are discretized into grids of size  $K_0$  each. Accordingly, the computational complexity of the coarse estimation of  $\phi_{\text{RB}}$  and  $\theta_{\text{BR}}$  are given by  $\mathcal{O}(TM_{\text{B}} M_{\text{R}} K_0)$  and  $\mathcal{O}(T^2 M_{\text{B}} K_0)$ , respectively. It is worthwhile mentioning that if we applied a simple 2D search, the computational complexity would have  $\mathcal{O}(TM_{\text{B}} M_{\text{R}} K_0^2)$ , having much more computational complexity compared with our approach. The computational cost of the refinement

TABLE I  
CONSIDERED SIMULATION PARAMETERS

Parameter	Symbol	Value
Wavelength	$\lambda$	1 cm
Light speed	$c$	$3 \times 10^8$ m/sec
Number of subcarriers	$N_c$	100
Number of transmissions	$T$	32
Sub-carrier spacing	$\Delta f$	120 kHz
Noise PSD	$N_0$	-174 dBm/Hz
RX's noise figure	$n_f$	5 dB
IFFT Size	$N_F$	1024
UE position	$\mathbf{p}_{\text{U}}$	$[6\text{m}, 6\text{m}]^{\top}$
BS position	$\mathbf{p}_{\text{B}}$	$[0\text{m}, 0\text{m}]^{\top}$
HRIS position	$\mathbf{p}_{\text{R}}$	$[2\text{m}, 10\text{m}]^{\top}$
RIS orientation	$\alpha$	$\pi/6$ rad
Number of BS antennas	$M_{\text{B}}$	17
Number of HRIS elements	$M_{\text{R}}$	33

of  $\phi_{\text{RB}}$  and  $\theta_{\text{BR}}$ , is given by  $\mathcal{O}(T^2 M_{\text{B}} I_0)$ , where  $I_0$  indicates the number of iterations. Similarly, the coarse and the fine estimation of  $\theta_{\text{BU}}$  have computational complexity with order  $\mathcal{O}(TM_{\text{B}}^2 K_0)$  and  $\mathcal{O}(TM_{\text{B}}^2 I_1)$ , respectively, where  $I_1$  shows the number of iterations. Besides, the computational complexity order of the coarse and the fine estimation of  $\theta_{\text{RU}}$  are given by  $\mathcal{O}(TM_{\text{B}}^2 M_{\text{R}}^2 K_0)$  and  $\mathcal{O}(TM_{\text{B}}^2 M_{\text{R}}^2 I_2)$ , respectively, where  $I_2$  shows the number of iterations. Overall, the complexity order of our estimator is  $C_o \approx \mathcal{O}(N_F \log(N_F)) + \mathcal{O}(T^2 M_{\text{B}} I_0) + \mathcal{O}(TM_{\text{B}}^2 I_1) + \mathcal{O}(TM_{\text{B}}^2 M_{\text{R}}^2 I_2)$ .

## IV. NUMERICAL RESULTS

In this section, we compare the root mean square error (RMSE)<sup>8</sup> of the estimated parameters with the corresponding CRBs<sup>9</sup> to evaluate the proposed estimator. For the RMSE calculations, we have averaged the results over 500 independent noise realizations. All the phase shifts of the HRIS elements have been drawn from the uniform distribution, i.e.,  $\angle[\gamma_t]_k \sim \mathcal{U}[0, 2\pi)$ . The same holds for the combiner vector at the HRIS, i.e.,  $\angle[\mathbf{c}_t]_i \sim \mathcal{U}[0, 2\pi)$ . The rest of the simulation parameters are given in Table I.

We first study the effect of the transmitted power  $P_t$  on the RMSE of the estimated parameters, as shown in Fig. 2(a)–(c). As can be seen, the RMSE of the estimations for the channel and the state parameters decreases as  $P_t$  increases, and the bounds for the channels parameters' estimations (i.e., BS-UE, BS-HRIS, BS-HRIS-UE) are attained when  $P_t = 0$  dBm and beyond. However, the RMSE of the BS-UE channel parameters' estimation deviates from its corresponding CRB when  $P_t > 5$  dBm. This happens because the error caused by noise is much smaller than that caused by the considered approximation at large  $P_t$  values, i.e., expression (13) becomes inaccurate. This implies that the larger  $P_t$  is, the higher the level of the reflected signals from the HRIS toward the UE is. It is shown in Fig. 2(b) that BS-HRIS-UE channel estimation does not show the degradation at high  $P_t$  that was observed in the BS-UE channel, although these two channels are coupled. This is because, even though there is a degradation in the BS-UE link, the

<sup>8</sup>We use the notations  $\sigma_{\text{R}}$  and  $\sigma_{\text{U}}$  for the RMSE of the HRIS position estimate  $\hat{\mathbf{p}}_{\text{R}}$  and the UE position  $\hat{\mathbf{p}}_{\text{U}}$ , respectively. The RMSE of the HRIS orientation estimation  $\hat{\alpha}$  is denoted by  $\sigma_{\alpha}$ , while  $\sigma_{\tau_{\text{BR}}}$ ,  $\sigma_{\tau_{\text{BU}}}$ , and  $\sigma_{\tau_{\text{BRU}}}$  are the RMSE of estimations of the parameters  $\hat{\tau}_{\text{BR}}$ ,  $\hat{\tau}_{\text{BU}}$ , and  $\hat{\tau}_{\text{BRU}}$ , respectively. Besides, The RMSE of the angle estimations  $\hat{\theta}_{\text{BR}}$ ,  $\hat{\theta}_{\text{BU}}$ ,  $\hat{\theta}_{\text{RU}}$ , and  $\hat{\phi}_{\text{RB}}$  are represented by  $\sigma_{\theta_{\text{BR}}}$ ,  $\sigma_{\theta_{\text{BU}}}$ ,  $\sigma_{\theta_{\text{RU}}}$ , and  $\sigma_{\phi_{\text{RB}}}$ , respectively.

<sup>9</sup>The CRBs corresponding to the estimations of the AoAs, AoDs, and ToAs, position and orientation are henceforth termed as AOA error bound (AAEB), AOD error bound (ADEB), TOA error bound (TEB), position error bound (PEB), and orientation error bound (OEB), respectively.

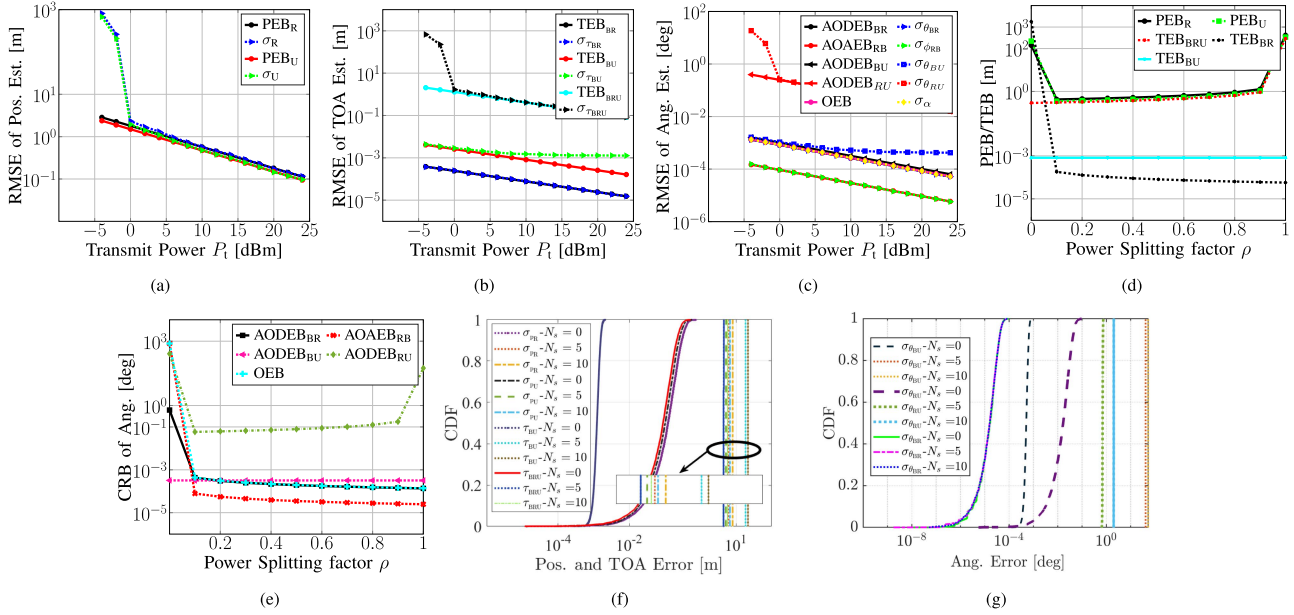


Fig. 2. Evaluation of the proposed estimator for the case where SPs are randomly distributed in  $[x, 5]$ , with  $x \sim \mathcal{U}(8, 13)$ , their radar cross section is  $0.1 \text{ m}^2$ , and the power splitting factor is set to  $\rho = 0.5$ . (a) The RMSE of the position estimations; (b) The RMSE of the ToAs estimations; (c) The RMSE of the AOA/AODs and RIS orientation estimations; (d) The effect of  $\rho$  on the TOA/positions estimations; (e) The effect of  $\rho$  on the angles (i.e., AoAs/AoDs and  $\alpha$ ) estimations; (f) The effect of the number of SPs around the UE on the estimation of the TOA and positions; and (g) The effect of the number of SPs around the UE on the estimation of the angles.

RMSE of the corresponding parameters is orders of magnitudes lower than the RMSEs in the BS-HRIS-UE link. Hence, the degradation in the BS-HRIS-UE link is negligible.

In Fig. 2(d) and (e), the effect of the common power splitting factor  $\rho$  on the estimation performance is assessed. As can be observed, as  $\rho$  increases (i.e., the sensing/reception power at the HRIS increases), the CRB of the BS-HRIS channel parameters' estimation decreases. We can see that the CRB of the HRIS rotation angle also decreases. This is due to the fact that the estimation of  $\alpha$  directly depends on the estimation of BS-HRIS channel parameters (i.e.,  $\hat{\theta}_{BR}$  and  $\hat{\phi}_{RB}$ ). Moreover, it is demonstrated that, as  $\rho$  increases, the estimation of the position of the HRIS and the UE exhibits a higher error variance, since these positions' estimations are coupled. Increasing the value of  $\rho$  leads to a decrease in the signal-to-noise ratio (SNR) at the UE. Accordingly, the UE cannot estimate the reflected channels, which contain joint information about the UE and the HRIS, with high accuracy. We also observe that when  $\rho \rightarrow 0$  and  $\rho \rightarrow 1$ , the estimations of both the BS-HRIS and HRIS-UE channel parameters fail. It can also be seen that  $\rho$  has no effect on the BS-UE channel estimation.

Besides, we depict the effect of SPs around HRIS on the proposed estimator accuracy in Fig. 2(f) and (g). Since similar algorithms are used for both BS-RIS and BS-UE channels, we only consider the SPs effect on the latter channel, when evaluating their effect on estimation accuracy using the approach of [11]. It can be seen that as the number  $N_s$  of SPs increases, the accuracy of the estimations deteriorates. Most of these deterioration are on  $\tau_{BU}$  and  $\theta_{BU}$ . That is because, according to our assumption, SPs directly affect BS-UE channel estimation and have no impact on other channels. Since the channel estimations are linked, the degradation of BS-UE channel estimation also affects the other channels' estimates. These impacts are not as pronounced as the direct impact of SPs on the BS-UE channel estimate. To tackle this issue, one solution can be the adoption of orthogonal profiles at the HRIS over time [12]; we leave this approach for future work.

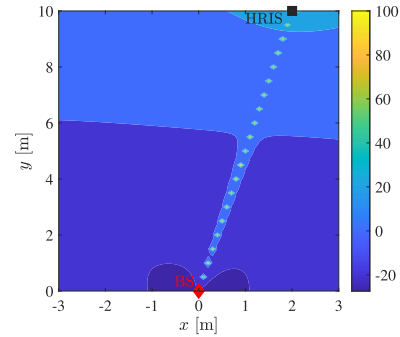


Fig. 3. Contour plot of the PEB (i.e.,  $10 \log_{10}(\text{PEB})$ ) versus the UE location for one random HRIS phase profile,  $P_t = 0 \text{ dBm}$ , and  $\alpha = 0^\circ$ .

Finally, we analyze the UE localization coverage and performance through a contour plot of the PEB in Fig. 3. As can be seen, highly accurate localization can be obtained when the UE is close to the BS due to high SNR. Furthermore, there are blind areas for the UE localization, where the UE is located on the connected line between the BS and the HRIS. Since BS, HRIS, and the UE do not build a triangle to exploit triangulation solution, see Section III-C.

## V. CONCLUSION

In this article, we presented a multi-stage estimator for the unknown location and orientation of a single-RX-RFC HRIS and the unknown position of a single-antenna UE in a multi-carrier system with a multi-antenna BS. The proposed estimation leverages the channel's geometrical features to estimate the targeted parameters. We showed that the RMSE of the estimations approaches the corresponding CRBs

within a certain SNR range. The simulation results also showed that selecting the HRIS power splitting ratio is critical to the estimation accuracy, and the effect of SPs should not be ignored. The formulated joint RIS calibration and user localization problem provides a practical solution for RIS-aided localization systems. In future work, 6D RIS calibration and 3D user positioning, HRIS phase profile optimization, multi-user cooperative calibration under LOS blockage, and mobile scenarios can be considered.

## REFERENCES

- [1] Q. Wu and R. Zhang, "Towards smart and reconfigurable environment: Intelligent reflecting surface aided wireless network," *IEEE Commun. Mag.*, vol. 58, no. 1, pp. 106–112, Jan. 2020.
- [2] E. Basar, M. Di Renzo, J. De Rosny, M. Debbah, M.-S. Alouini, and R. Zhang, "Wireless communications through reconfigurable intelligent surfaces," *IEEE Access*, vol. 7, pp. 116753–116773, 2019.
- [3] S. Hu, F. Rusek, and O. Edfors, "Beyond massive MIMO: The potential of positioning with large intelligent surfaces," *IEEE Trans. Signal Process.*, vol. 66, no. 7, pp. 1761–1774, Apr. 2018.
- [4] D. Dardari, "Communicating with large intelligent surfaces: Fundamental limits and models," *IEEE J. Sel. Areas Commun.*, vol. 38, no. 11, pp. 2526–2537, Nov. 2020.
- [5] Y. Liu et al., "Reconfigurable intelligent surfaces: Principles and opportunities," *IEEE Commun. Surveys Tuts.*, vol. 23, no. 3, pp. 1546–1577, thirdquarter 2021.
- [6] W. Saad, M. Bennis, and M. Chen, "A vision of 6G wireless systems: Applications, trends, technologies, and open research problems," *IEEE Netw.*, vol. 34, no. 3, pp. 134–142, May/Jun. 2020.
- [7] O. Rinchi, A. Elzanaty, and M.-S. Alouini, "Compressive near-field localization for multipath RIS-aided environments," *IEEE Commun. Lett.*, vol. 26, no. 6, pp. 1268–1272, Jun. 2022.
- [8] S. Huang, B. Wang, Y. Zhao, and M. Luan, "Near-field RSS-based localization algorithms using reconfigurable intelligent surface," *IEEE Sensors J.*, vol. 22, no. 4, pp. 3493–3505, Feb. 2022.
- [9] A. Elzanaty, A. Guerra, F. Guidi, and M.-S. Alouini, "Reconfigurable intelligent surfaces for localization: Position and orientation error bounds," *IEEE Trans. Signal Process.*, vol. 69, pp. 5386–5402, 2021.
- [10] K. Keykhosravi, M. F. Keskin, G. Seco-Granados, and H. Wymeersch, "SISO RIS-enabled joint 3D downlink localization and synchronization," in *Proc. IEEE Int. Conf. Commun.*, Montreal, Canada, 2021, pp. 1–6.
- [11] K. Keykhosravi, M. F. Keskin, S. Dwivedi, G. Seco-Granados, and H. Wymeersch, "Semi-passive 3D positioning of multiple RIS-enabled users," *IEEE Trans. Veh. Technol.*, vol. 70, no. 10, pp. 11073–11077, Oct. 2021.
- [12] K. Keykhosravi, M. F. Keskin, G. Seco-Granados, P. Popovski, and H. Wymeersch, "RIS-enabled SISO localization under user mobility and spatial-wideband effects," *IEEE J. Sel. Topics Signal Process.*, vol. 16, no. 5, pp. 1125–1140, Aug. 2022.
- [13] C. Pan et al., "An overview of signal processing techniques for RIS/IRS-aided wireless systems," *IEEE J. Sel. Topics Signal Process.*, vol. 16, no. 5, pp. 883–917, Aug. 2022.
- [14] M. Jian et al., "Reconfigurable intelligent surfaces for wireless communications: Overview of hardware designs, channel models, and estimation techniques," *Int. Conv. Netw.*, vol. 3, no. 1, pp. 1–32, Mar. 2022.
- [15] G. C. Alexandropoulos et al., "Hybrid reconfigurable intelligent metasurfaces: Enabling simultaneous tunable reflections and sensing for 6G wireless communications," 2021, *arXiv:2104.04690*.
- [16] H. Wymeersch, J. He, B. Denis, A. Clemente, and M. Juntti, "Radio localization and mapping with reconfigurable intelligent surfaces: Challenges, opportunities, and research directions," *IEEE Veh. Technol. Mag.*, vol. 15, no. 4, pp. 52–61, Dec. 2020.
- [17] G. C. Alexandropoulos et al., "Localization via multiple reconfigurable intelligent surfaces equipped with single receive RF chains," *IEEE Wireless Commun. Lett.*, vol. 11, no. 5, pp. 1072–1076, May 2022.
- [18] R. Ghazalian, I. Vinieratou, and H. Wymeersch, "Bi-static sensing for near-field RIS localization," in *Proc. IEEE Glob. Commun. Conf.*, 2022, pp. 6457–6462.
- [19] J. He, H. Wymeersch, and M. Juntti, "Channel estimation for RIS-aided mmWave MIMO systems via atomic norm minimization," *IEEE Trans. Wireless Commun.*, vol. 20, no. 9, pp. 5786–5797, Sep. 2021.
- [20] G. C. Alexandropoulos and E. Vlachos, "A hardware architecture for reconfigurable intelligent surfaces with minimal active elements for explicit channel estimation," in *Proc. IEEE Int. Conf. Acoust., Speech, Signal Process.*, 2020, pp. 9175–9179.
- [21] Y. Han, S. Jin, J. Zhang, J. Zhang, and K.-K. Wong, "DFT-based hybrid beamforming multiuser systems: Rate analysis and beam selection," *IEEE J. Sel. Topics Signal Process.*, vol. 12, no. 3, pp. 514–528, Jun. 2018.